Quantitative Analysis of Three-Dimensional-Resolved Fiber Architecture in Heterogeneous Skeletal Muscle Tissue Using NMR and Optical Imaging Methods

Vitaly J. Napadow,* Qun Chen,† Vu Mai,† Peter T. C. So,* and Richard J. Gilbert*
*Department of Mechanical Engineering and Center for Biomedical Engineering, Massachusetts Institute of Technology, Cambridge; and †Department of Radiology, Beth Israel Deaconess Medical Center and Harvard Medical School, Boston, Massachusetts

ABSTRACT The determination of principal fiber directions in structurally heterogeneous biological tissue substantially contributes to an understanding of its mechanical function in vivo. In this study we have depicted structural heterogeneity through the model of the mammalian tongue, a tissue comprised of a network of highly interwoven fibers responsible for producing numerous variations of shape and position. In order to characterize the three-dimensional-resolved microscopic myoarchitecture of the intrinsic musculature of the tongue, we viewed its fiber orientation at microscopic and macroscopic length scales using NMR (diffusion tensor MRI) and optical (two-photon microscopy) imaging methods. Diffusion tensor imaging (DTI) of the excised core region of the porcine tongue resulted in an array of 3D diffusion tensors, in which the leading eigenvector corresponded to the principal fiber orientation at each location in the tissue. Excised axially oriented lingual core tissues (fresh or paraffin-embedded) were also imaged with a mode-locked Ti-Sapphire laser, (76 MHz repetition rate, 150 femtosecond pulse width), allowing for the visualization of individual myofibers at in situ orientation. Fiber orientation was assessed by computing the 3D autocorrelation of discrete image volumes, and deriving the minimal eigenvector of the center voxel Hessian matrix. DTI of the fibers, comprising the intrinsic core of the tongue, demonstrated directional heterogeneity, with two distinct populations of fibers oriented orthogonal to each other and in-plane to the axial perspective. Microscopic analysis defined this structural heterogeneity as discrete regions of in-plane parallel fibers, with an angular separation of ~80°, thereby recapitulating the macroscopic angular relationship. This analysis, conceived at two different length scales, demonstrates that the lingual core is a spatially complex tissue, composed of repeating orthogonally oriented and in-plane fiber patches, which are capable of jointly producing hydrostatic elongation and displacement.

INTRODUCTION

The mechanical properties of skeletal muscle are dictated largely by the distribution and spatial orientation of its constituting fibers. While the determination of principal fiber direction is relatively straightforward in homogeneous tissues, the fibers of which are largely aligned along a single spatial axis, the process is considerably more complicated in heterogeneous tissues, the fibers of which are aligned along multiple spatial axes. The analysis of fiber populations within such complex fiber arrays requires a quantitative method capable of resolving principal fiber direction in three dimensions at varying length scales.

In order to develop an analytic approach to resolve such complex fiber populations, we employed the model of the mammalian tongue, one of the most elegant living models of structural heterogeneity. The tongue is an intricately configured muscular organ that has paramount importance during diverse physiological functions, such as swallowing, speech, and prey capture. The intrinsic myoarchitecture of the tongue (those fibers having no extrinsic attachments) may be characterized as a core region of muscle fibers, aligned perpendicular to the long axis of the tongue, contained within a sheath-like tract of longitudinally oriented fibers (Miyawaki, 1974). The intrinsic fibers are merged with extrinsic muscles (those fibers originating at bony attachments), and modify the shape and position of the tongue from the superior, posterior, and inferior directions. The organization of the intrinsic core fibers has particular importance because patterned contraction of these muscles are believed to produce not only tissue displacement, but also functional reconfiguration of the spatially dependent material properties of the tissue.

We have previously studied three-dimensional lingual myoarchitecture in the intact tongue with diffusion-weighted NMR techniques, i.e., diffusion tensor imaging (DTI) (Gilbert et al. 1998; Wedeen et al., 2001). This technique measures spatially variant proton self-diffusivity, producing a diffusion tensor field, which is spatially resolved on the order of a mm^3 voxel. Due to the increased hindrance of diffusion in directions orthogonal to the myofiber axis, these data provide information regarding the direction (principal eigenvector of the diffusion tensor) and degree of alignment (diffusion anisotropy) of the constituting mean fiber population (Le Bihan, 1995; van Doorn et al. 1996; Basser 1995). Thus, homogeneously aligned muscle fiber organization may be inferred by high diffusion anisotropy, whereas heterogeneous alignment of the constituting fibers can be inferred by lower diffusion anisotropy. With this method, we observed that the lingual core was a region of low diffusion anisotropy (compared to the sheath), sug-

Received for publication 1 March 2000 and in final form 19 March 2001.
Address reprint requests to Richard J. Gilbert, MD, Massachusetts Institute of Technology, 77 Massachusetts Avenue, Cambridge, MA 02139. Phone: 617-254-6875; Fax: 617-254-6978; E-mail: rgilbert@mit.edu.

0006-3495/01/06/2968/08 $2.00

gesting that fiber content within the voxel was not aligned as parallel fibers but rather as a combination of heterogeneously oriented fiber populations. This was contrasted with the high diffusion anisotropy of the intrinsic sheath and extrinsic muscles, indicating a parallel alignment of the constituting fibers. However, mechanical analysis of the core fibers during certain motions, such as swallowing (Miller 1982), suggest that these fibers may undergo spatially variant activation (Napadow, et al., 1999, a, b). Thus, there is a strong rationale for considering fiber architecture resolved to the level of the individual fiber or grouped fiber bundles, which can be conceived at all relevant spatial dimensions.

Two-photon excitation microscopy may constitute an optimal method for visualizing in situ fiber architecture due to its ability to scan a three-dimensional tissue space with laser excitation configured to excite two (or more) photons at discrete locations in the tissue (Denk et al., 1990, Centonze et al., 1998; Masters et al., 1997). The particular applicability of two-photon microscopy for depth discrimination in thick tissues results from the fact that fluorescence signal intensity is highly dependent on the degree of photon flux, which decreases rapidly as a function of distance from the focal plane. In this study, we have used the combination of NMR (diffusion tensor MRI) and optical (two-photon excitation microscopy) techniques to interrogate the microstructure of the core fibers of the mammalian tongue, and have developed an analytic framework that conceives of three-dimensional microstructure on the basis of both its local diffusivity and its explicit micro-anatomical patterns.

METHODS

Specimens

Two-photon excitation microscopy and DTI were performed on three excised porcine tongues obtained from Blood Farms (West Groton, MA). The tongue was excised by making an incision from the thyroid prominence to the angle of the mandible, in order to expose the tongue, followed by en bloc resection. Whole tongue specimens were refrigerated and scanned within 24 h of harvest. For microscopy, tissue specimens ($20 \times 20 \times 8$ mm) were obtained from core of the anterior region of the tongue, visually localized to correspond to the region from which diffusion tensor data was acquired. The tissue specimens for three-dimensional microscopy were either fixed (10% gluteraldehyde) and embedded in paraffin, or viewed as fresh tissue, without fixation. In addition, in the case of the fixed tissue, following 3D microscopy the tissue was sliced with a microtome (Olympus) to a thickness of 0.4 μm, stained with either hematoxylin and eosin (H&E) or trichome, and viewed with conventional light microscopy.

Diffusion tensor imaging

Diffusion tensor imaging was performed on whole porcine tongue specimens with a 1.5T Siemens Vision System equipped with head coil. A double-echo EPI sequence was utilized (TR/TE = 5000/100 ms) with an image matrix of 96×128, corresponding to a phase-encoded interpolated voxel resolution of $1.95 \times 1.95 \times 8.00$ mm. A double-echo sequence was utilized to limit image artifact produced by deleterious eddy currents resulting from gradient switching (Reese, Weisskoff et al., 1998) and to increase the b-value to 620 s/mm^2 (gradient strength = 18 mT/m, Δ_1 = 15.79 ms, Δ_2 = 14.47 ms, Δ_3 = 15.79 ms, δ = 12.67 ms).

Diffusion tensor imaging was employed to characterize proton diffusion (as free water) in the anisotropic medium of skeletal muscle. In spin-echo diffusion-weighted MR images, molecular displacements result in the attenuation of the refocused spin echo; thus, NMR signal attenuation increases with increased molecular displacement. Diffusion sensitization can be achieved in 3D space by varying the orientation of the diffusion gradients in the MR pulse sequence. Hence the diffusion tensor can be conceived as a function of signal attenuation as:

$$\ln\left(\frac{S_b}{S_0}\right) = -\sum_{i=1}^{3}\sum_{j=1}^{3} b_{ij} D_{ij}$$

where S_b is the signal attenuated image, S_0 is the unattenuated image, b_{ij} is the ij component of the classic b-matrix, and D_{ij} is the ij component of the diffusion tensor (Basser 1995). The b-matrix is related to the direction dependent diffusion sensitization and is expressed as:

$$\mathbf{b} = \int \mathbf{k}^T \mathbf{k} dt$$

where the reciprocal space vector, $\mathbf{k}$, can be expressed as a function of the proton gyromagnetic ratio, γ, and the 3D diffusion sensitization gradient vector, $\mathbf{G}$

$$\mathbf{k} = \gamma \int \mathbf{G} dt$$

In order to efficiently span 3D space with the diffusion sensitization gradients, seven images were acquired; six with gradient vectors toward the unopposed edge centers of a theoretical cube, and one unattenuated ($\mathbf{G}$ = 0) image.

The complete 3D diffusion tensor was computed for each image voxel and was visualized as individual octahedra, whose axes were scaled by the size of the eigenvalues and oriented along the corresponding eigenvectors. The octahedra were color-coded based on the principal eigenvector {x, y, z} triplet mapped to the red-green-blue color-space. Mean fiber orientation was deduced from the images by computing the principal eigenvector of the diffusion tensor. Only voxels with significant fiber content (i.e., anisotropy index as ratio of eigenvalues $\lambda_1/\lambda_2 > 1.15$) were included in the analysis. A total of n = 15 tensors were analyzed for correlation with two-photon microscopy. The mean fiber orientation for each voxel was calculated and the data presented as a cubic spline-smoothed polar histogram plot.

Two-photon excitation microscopy

We used two-photon excitation microscopy (excitation wavelength, 780 nm) to image lingual muscle fiber autofluorescence in vivo. Tissue specimens were imaged with a mode-locked Ti-sapphire laser, with a 76-MHz repetition rate and a 150-femtosecond pulse width (Coherent, Inc., Palo Alto, CA). The power of the laser light source was regulated to ~130 mW with a Glan-Thompson polarizer, which, given a transmission efficiency of 10 to 20%, resulted in ~15 mW at the level of the muscle tissue. The beam expanded laser light was directed into the microscope via a galvanometer-driven x-y scanner (Cambridge Technology, Watertown, MA), and images were generated by raster scanning the x-y mirrors. The excitation light entered the microscope via a modified epifluorescence light pathway, while the scan lens was positioned such that the x-y scanner was at its eye-point while the field aperture was at its focal point. The axial position of the objective was driven by a piezoelectric driver, with a resolution of 0.05 μm over 100 μm. The typical frame rate (per single image slice) was ~3 s.

In order to maximize the number of available photons for detection (while minimizing potential photo-damage), we used a single photon counting system in which the fluorescence signal at each pixel was de-

tected by an R5600-P photo-multiplier tube (Hamamatsu, Bridewater, NJ). This constitutes a photon counting module with high quantum efficiency (12% at 500 nm and 25% at 400 nm). A 100-MHz single photon counting discriminator (F100T, Advanced Research Instruments, Boulder, CO) converted single photon bursts into TTL pulses, which were subsequently counted and saved on a PC computer (Gateway) as photon intensity modulated images. The 3D deep-tissue volume scans, based on a Zeiss 10× (0.5 N.A.) objective, produced 256 × 256 images with resolution 1.85 × 1.85 μm and a slice thickness of 5 μm. We have chosen a relatively coarse resolution in this study to maximize the achievable field of view. Because the tissue volume was sampled at a low resolution, a potential concern is that the measured periodicity of the fiber structures may be distorted due to aliasing. To assured that no such aliasing is present, we also imaged the same tissue using a higher N.A. objective (Zeiss Fluar 40X, 1.2 N.A., results not shown). Using this higher N.A. objective, we can achieve radial and axial resolutions of 0.3 μm and 0.5 μm, respectively. Under these conditions, no higher spatial frequency muscle fiber structures were observed. Further, our choice of imaging resolution is also consistent with known tissue anatomy. Skeletal muscles cells typically have a lateral dimension of 30 to 50 μm and axial length of over 1 mm, dimensions which are significantly larger than the chosen imaging resolution. The achievable scan depth was ~100 μm.

Two-photon microscopy image processing

Image processing was achieved via a 3D autocorrelation algorithm. The autocorrelation of an image volume (or subvolume) is computed in order to find average repetitive structures within the image (Russ 1999), such as homogeneously aligned fibers. Practically speaking, the Fourier transform of the image volume is multiplied by its own complex conjugate and the result inverse-transformed back to real space.

$$ACorr(g(t))_j = \int_{-\infty}^{\infty} g(\tau)g(t+\tau)dt = IFFT(G_k G_k^*)$$

where g_j is the real space image volume, and G_k is its Fourier transform. The asterisk denotes complex conjugation. Before transformation, image volumes were interpolated in the through plane dimension and windowed with a Kaiser window. The former procedure was implemented because the data volume was originally spatially anisotropic, while the latter procedure accounted for the lack of periodicity in the data (i.e., no wraparound at the edges).

The center of the autocorrelation volume contains a 3D intensity distribution, which is aligned in space according to the alignment of the mean fiber populations within the original image volume. In order to compute this orientation, we calculated the Hessian matrix at the center voxel of the autocorrelation volume:

$$\mathbf{H} = \begin{bmatrix} I_{xx} & I_{xy} & I_{xz} \\ I_{yx} & I_{yy} & I_{yz} \\ I_{zx} & I_{zy} & I_{zz} \end{bmatrix}$$

Discrete derivatives were computed with a higher order five-point scheme with error $O(h^4)$. The eigensystem of the Hessian was then found and the eigenvector corresponding to the smallest eigenvalue (in absolute value) conferred the direction of lowest curvature, which by extension is the mean 3D fiber orientation within the sampled image subvolume.

Two-photon image datasets (n = 5) were first filtered with blind deconvolution to correct for asymmetric excitation point-spread function (AutoDeblur; AutoQuant Imaging Inc., Watervliet, NY). This dataset was then divided into 50 × 50 × 9 voxel subvolumes, which were analyzed by the previously described autocorrelation algorithm. A total of n = 63 subvolumes were analyzed and data was presented with a cubic spline-smoothed polar histogram plot. This plot was then qualitatively compared to the corresponding plot generated by the DTI analysis.

RESULTS

Fig. 1 depicts a diffusion tensor image of an axial slice of the porcine tongue. The diffusion tensors are shown as an octahedron oriented along the eigenvectors of the diffusion tensor, and color-coded according to the orientation of the principal eigenvector. Diffusion tensor imaging of the tongue revealed a core region of in-plane fibers oriented approximately orthogonal to each other, and a region of longitudinally oriented fibers principally in the periphery (Fig. 1 *A*). Analysis of the sub-region, which was subsequently sampled with two-photon microscopy, is shown in

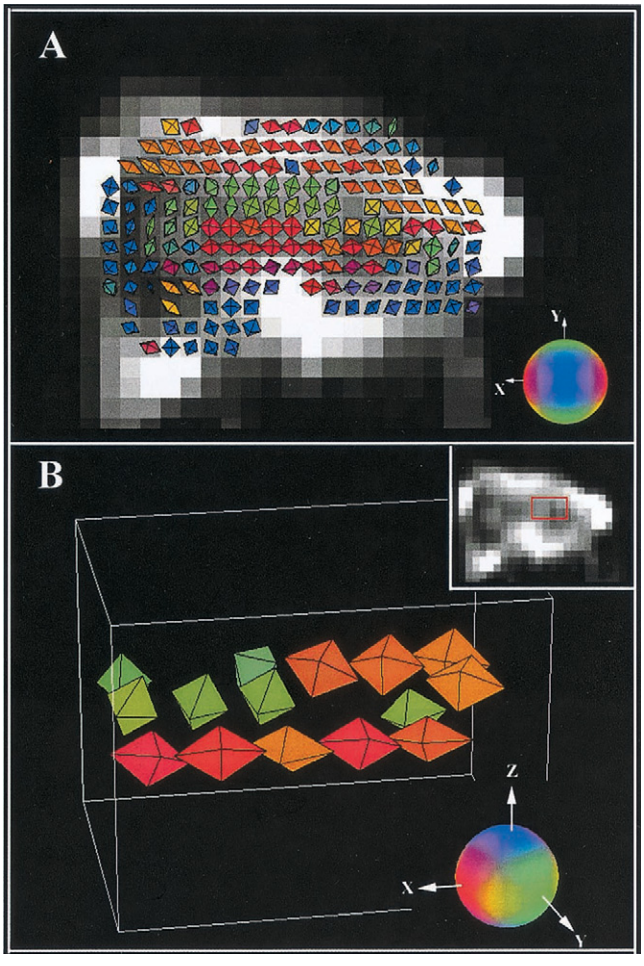

FIGURE 1 DTI of an axial slice of the porcine tongue. The diffusion tensors are shown as octahedra oriented along the eigenvectors of the diffusion tensor, and color-coded according to the orientation of the principal eigenvector. (*A*) the entire axial slice being composed of a core region of in-plane fibers oriented approximately orthogonal to each other (*red* and *green*) corresponding to the verticalis and transversus muscle, and a region of longitudinally oriented fibers principally in the periphery (*blue*). (*B*) the region later sampled with two-photon microscopy which also shows orthogonally oriented fiber populations (*red* and *green*), mostly in-plane to the imaging slice.

Fig. 1 *B*. This sub-region contained octahedra that toggled between a medial-lateral and superior-inferior orientation.

The 3D distribution of individual myofibers within the lingual core was visualized with two-photon excitation microscopy (Fig. 2) utilizing the autofluorescence of fixed tissue specimens. In contrast, fresh tissue did not produce sufficient autofluorescence to allow adequate single fiber discrimination. Volume content determined by two-photon microscopy was compared to a histological assessment of similar tissue using H&E. Trichrome stains (not shown) confirmed that the imaged structures were principally skeletal muscle, with minimal collagen. Mean 3D-fiber orientation within the two-photon datasets was computed with an autocorrelation algorithm. A sample image and its 3D autocorrelation volume is presented in the xy, xz, and yz projections, with the computed orientation vector superimposed (Fig. 3).

Quantitative data analysis from the DTI ($n = 15$) and two-photon microscopy ($n = 63$) datasets are depicted in Table 1. Both DTI and two-photon microscopy exhibited two distinct fiber populations. By DTI, one composite fiber population was oriented in-plane at $-16.8°$ relative to the horizontal, while another composite fiber population was oriented at 65.4°, yielding a relative in-plane fiber angle of 82.2°. Similarly, the transversus muscle fiber population was found with two-photon microscopy to be oriented in-plane at 3.6° relative to the horizontal, while the verticalis muscle fiber population was oriented at 84.0°, corresponding to a relative in-plane fiber angle of 80.4°. Moreover, sampling from both DTI and two-photon microscopy supported the consistently in-plane fiber orientation of the anterior tongue core, as mean through-plane angle was 1.3° ($\sigma = 9.4°$) and $-0.3°$ ($\sigma = 5.1°$), respectively.

DISCUSSION

The understanding of mechanical function in complex fiber systems is largely dependent upon the ability to extract

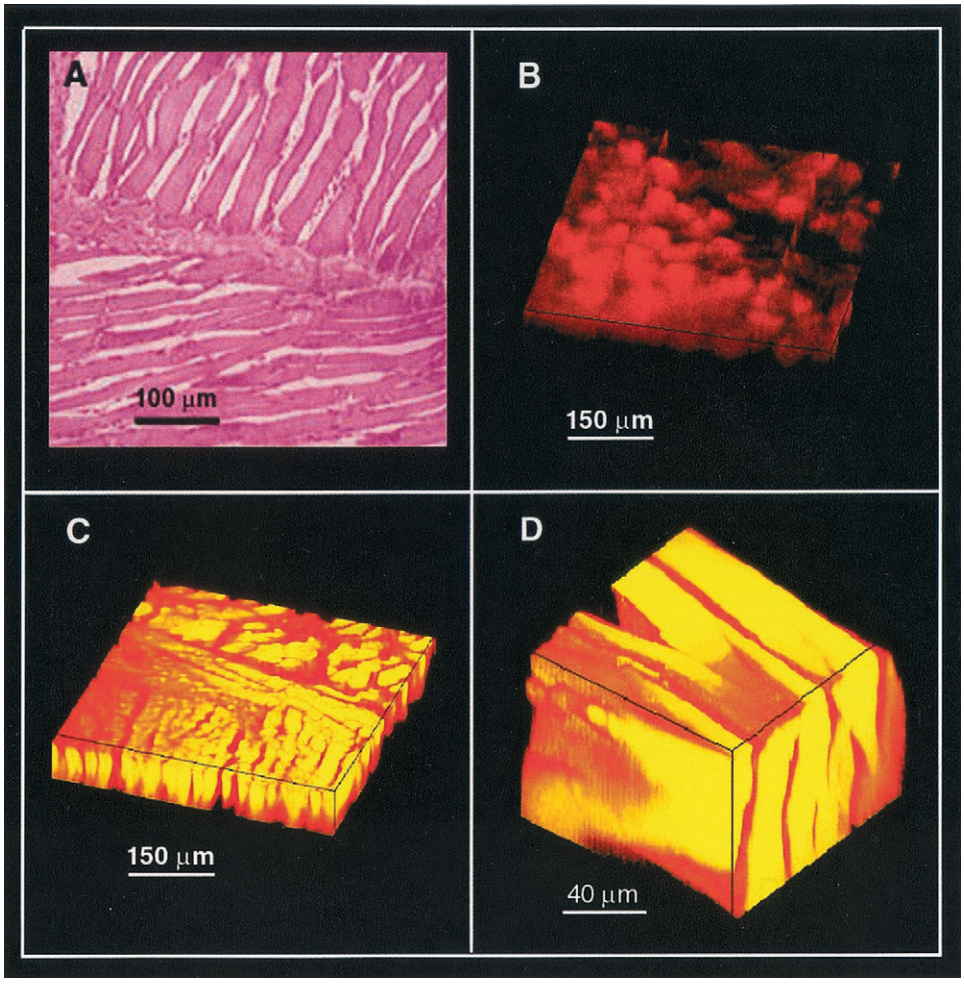

FIGURE 2 Two-photon microscopy of the anterior core region of the porcine tongue. The 3D distribution of individual myofibers within the lingual core was visualized with two-photon excitation microscopy utilizing fixed tissue specimens (*C*, ×100; *D*, ×400). In contrast, fresh tissue did not produce sufficient autofluorescence to allow adequate single fiber discrimination (*B*). Volume content determined by two-photon microscopy was compared to a histological assessment of the same tissue using H&E (Fig. 2 *A*, ×100). The secondary organization of the lingual core myofibers into a patchwork of fiber bundles can be seen in *A* and *C*.

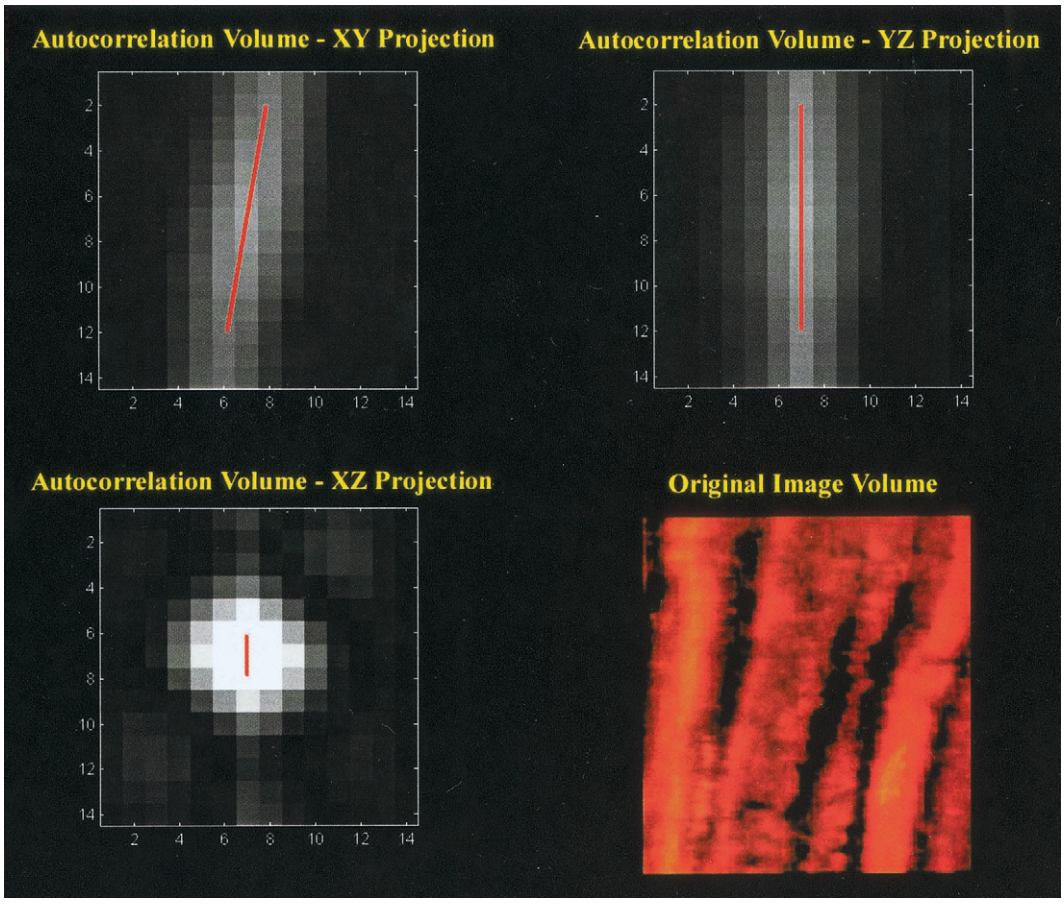

FIGURE 3 Three-dimensional fiber orientation as computed by an autocorrelation algorithm. Mean 3D fiber orientation within the two-photon data sets was computed with an autocorrelation algorithm. (*D*) a sample image subvolume on end. (*A–C*) the 3D autocorrelation volume of the subvolume presented in *xy*, *xz*, and *yz* projections, with the computed orientation vector superimposed (*red*).

information regarding principal fiber direction in these tissues. Owing to its highly interwoven fiber anatomy, the mammalian tongue may be a suitable model to develop analytic models for fiber direction in heterogeneous biological tissues. In this study, we have employed NMR and optical techniques to image intramural structures, thus conceiving fiber direction at varying length scales in the same tissue.

The mammalian tongue is believed to function as a muscular hydrostat, an organ the musculature of which both creates motion and supplies skeletal support for that motion (Smith and Kier, 1989). As such, it capitalizes on its high water content, and hence incompressibility, to impose functional elongation along directions orthogonal to directions of muscular contraction. In this regard, the tongue can be considered analogous to other muscular hydrostats in nature, such as the elephant trunk and squid tentacle, which are composed almost entirely of muscle and devoid of calcified internal or external skeletal elements. The hydrostatic properties of the mammalian tongue may be attributed to the coordinated contractions of the intrinsic muscle fiber arrays (i.e., transversus and verticalus muscles) in the core region of the tissue. A long-standing biological conundrum has been the inability to explain how the anatomical distribution of these lingual fibers contributes to the explicit set of deformations required for physiological motion.

Our results confirm the classical anatomical description of the lingual core as two distinct in-plane fiber populations, specifically the intrinsic transversus and verticalis muscles. Based on DTI, we discerned a near orthogonal angular separation between these fiber populations. This orthogonal relationship was recapitulated at the microscopic level, thus indicating that the orthogonal relationship between fiber or fiber bundles exists as a repeating event throughout the tissue. Through two-photon microscopic imaging, we were able to discriminate the explicit 3D structural basis for the orthogonal fiber relationship. As shown in Fig. 2, the fibers in the lingual core region were not, in fact, aligned as interwoven individual fibers, but rather were organized into fiber bundle sheets. The composition of the mammalian tongue core is likely to incorporate serially alternating sheets of transversus muscle and verticalis muscle, which, at least in the case of the canine tongue, traverse the entire intrinsic core region (Mu and Sanders, 1999). The exact size

TABLE 1 Data analysis from computed DTI and two-photon microscopy myofiber orientations

Fiber population	Mean	Standard deviation
Diffusion tensor imaging (n = 15)		
Composite fiber population 1 in-plane angle (n = 9)	−16.8°	13.8°
Composite fiber population 2 in-plane angle (n = 6)	65.4°	5.7°
Relative angular separation	82.2°	
Combined through-plane angle (n = 15)	1.3°	9.4°
Two-photon microscopy (n = 63)		
Transversus muscle in-plane angle (n = 35)	3.6°	15.4°
Verticalis muscle in-plane angle (n = 28)	84.0°	10.2°
Relative angular separation	80.4°	
Combined through-plane angle (n = 63)	−0.3°	5.1°

Quantitative data analysis from the diffusion tensor imaging (n = 15) and two-photon microscopy (n = 63) datasets is presented as a table of in-plane and through-plane angle. Both diffusion tensor imaging and two-photon microscopy exhibited two distinct fiber populations, one corresponding to transversus m. and the other to verticalis m., both intrinsic muscles of the tongue core. Relative in-plane fiber angle found with DTI was 82.2°. Similarly, the relative in-plane fiber angle found with two-photon microscopy was 80.4°. Sampling from both diffusion tensor imaging and two photon microscopy supported the consistently in-plane fiber orientation of the anterior tongue core, as mean through-plane angle was 1.3° (σ = 9.4°) and −0.3° (σ = 5.1°), respectively.

and geometry of the bundles cannot be determined from our data since the slicing technique allowed for the possibility that a given axial slice holds any number of verticalis or transversus bundles. We speculate that similarly oriented bundles may either act *en masse* as distinct contractile units, or serve to localize a portion of a fiber population's fibers into a specific region so that regional contraction employs fibers from different fiber populations. During physiological motions, the efficient execution of different lingual tasks most likely employs a combination of both these strategies. In human swallowing, for instance, serially alternating transversus and verticalis bundles may allow for the bolus accommodating depression in the tissue to translate posteriorly, bringing food deeper into the oropharynx. Both fiber types are necessary as verticalis muscle contraction allows for a depression to be formed, while transversus muscle contraction creates expansion toward the hard palate, following the principles of a muscular hydrostat. (Napadow et al., 1999a).

Fiber orientation, conceived at a macroscopic level through depiction of the NMR diffusion tensor, differs fundamentally from the determination of fiber orientation, conceived at a microscopic level through two-photon microscopy. In the case of NMR DTI, since the two fiber populations of the lingual core were nearly orthogonal to one another, and the b-value employed was relatively low, the principal eigenvector of the diffusion tensor tended to alternate between two orientations (Fig. 1). The low anisotropy present in the sampled voxels confirmed the existence of more than one fiber population (Wedeen et al., 2001). Furthermore, with two-fiber populations, estimating fiber orientation with a single second-order tensor will produce a result somewhere in between the two populations, as the NMR signal with diffusion equation is based on a nonlinear summation of the two populations, under the slow exchange hypothesis:

$$\frac{S_1}{S_0} = f_1 e^{-k_1^{\mathrm{T}}\mathbf{D}_1 k_1 \tau} + f_2 e^{-k_1^{\mathrm{T}}\mathbf{D}_2 k_1}$$

where S_1 denotes the NMR echo peak intensity corresponding to the gradient direction given by $\mathbf{k}_1$ (one of six different gradient directions), S_0 denotes the intensity without a diffusion sensitization gradient. f_1 and f_2 denote the respective fiber fractions of the two populations ($f_1 + f_2 = 1$), $\mathbf{k}_1$ is the spatial modulation vector given by $\mathbf{k}_1 = 2\pi\gamma_{\mathrm{H}} t_{\mathrm{d}} G_1$ (γ_{H} is the proton gyromagnetic ratio, t_{d} is the diffusion time, and $\mathbf{G}_1$ is the magnetic field gradient. $\mathbf{D}_{\mathrm{i}}$ is the second-order diffusion tensor corresponding to the i^{th} fiber population and τ denotes the diffusion sensitization gradient spacing for a classic two gradient experiment. For the purposes of the DTI experiment, if a tissue is modeled with two fiber populations (equal fiber fraction) that are oriented 80° apart, the standard seven-point diffusion tensor experiment would predict a diffusion tensor the principal eigenvector of which was 40° deviated from the nearest actual fiber population (Fig. 4). DTI thus predicts a fiber population between the two actual fiber populations, with maximal signal attenuation attributed to diffusion sensitization occurring approximately in the middle of the two actual fiber populations. An explicit correction to the DTI data could indeed be made if both fiber fraction and relative angular orientation were known for every voxel sampled. However, as this information is unknown, it must be stressed that only the plane in which the two actual fiber populations lie can be definitively deduced from the DTI data; it is the plane defined by the first two tensor eigenvectors and was found to be in-plane. Furthermore, the reason that the principal eigenvector of the diffusion tensor toggles between two distinct states was due, serendipitously, to the near orthogonal nature of the two actual fiber populations. Because the diffusion tensor's principal eigenvector will nearly bisect the acute angle formed by the fiber crossing, the Cartesian quadrant in which that eigenvector will land is dependent on the quadrant in which the acute angle of the fiber crossing is located. That is, if the transversus muscle is defined to lie along the x axis in a standard Cartesian x-y coordinate system, and the verticalis muscle is at 80°, the bisected angle will be 40°. However, if that verticalis muscle population is now at 100° (note that the fiber crossing angle would still be the acute 80° angle), the bisected angle along which the diffusion tensor's principal eigenvector now lies would be 140°. In fact, a singularity exists if the fiber crossing angle is exactly 90° (Fig. 4). We believe that this phenomenon explains the toggling nature of the octahedra in our DTI data.

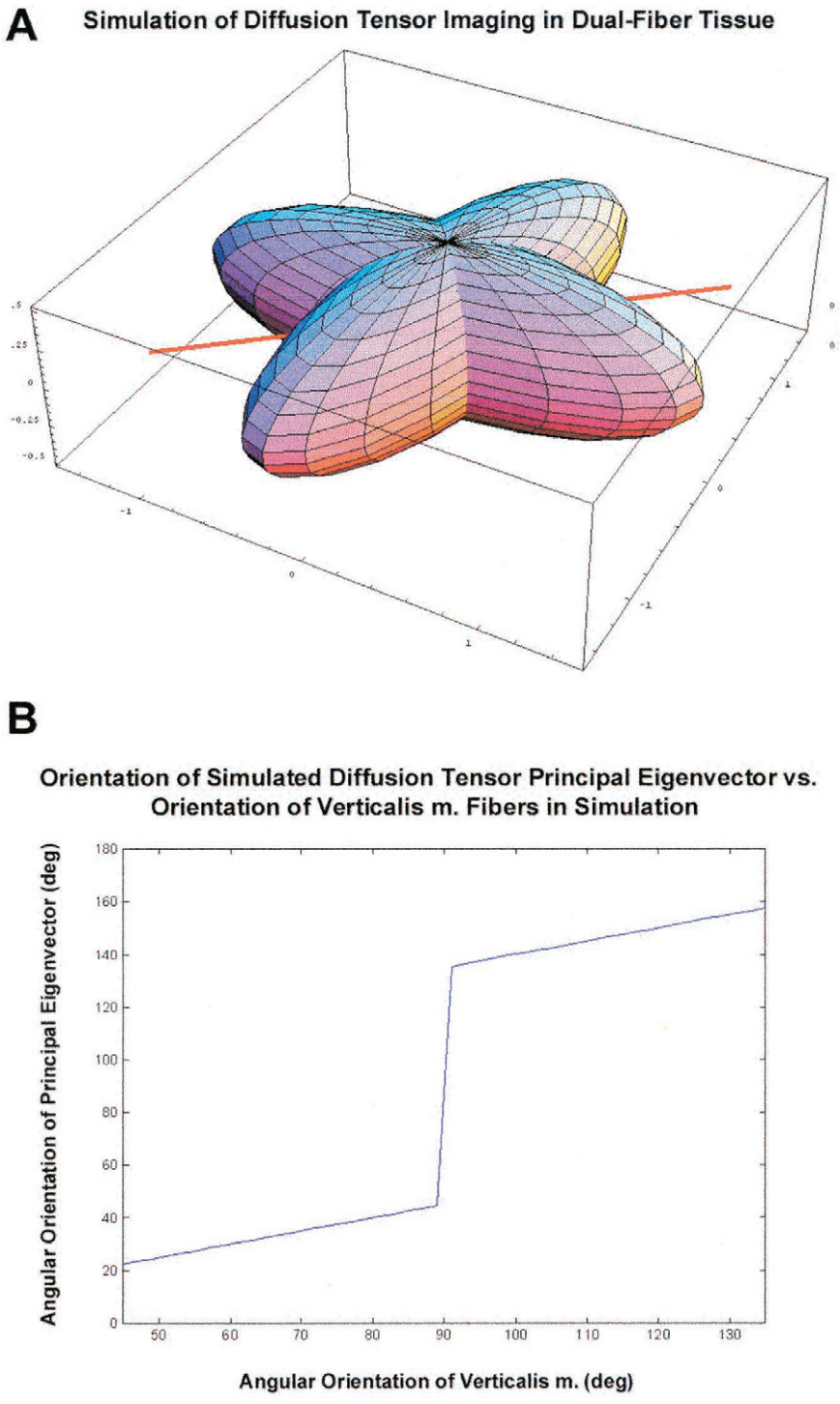

FIGURE 4 Computer simulation showing error in using DTI to calculate fiber direction for tissue with multiple fiber populations. (*A*) Computer modeling of two equally distributed fiber populations oriented 80° apart in-plane (comparable to actual tongue core tissue as visualized with two-photon microscopy), in accordance with a standard seven-sample DTI experiment. Each actual fiber population was modeled by a single diffusion tensor ellipsoid (seen in the figure) whose principal eigenvalue was three times greater than the second or third eigenvalue. Setting the sum of these two exponentials (defining NMR signal intensity corresponding to the two populations) equal to the signal due to a single composite diffusion tensor (that which would be measured by the DTI experiment), a system of nonlinear equations could be solved for the composite tensor. The principal eigenvector of this predicted diffusion tensor is represented by the red line segment. If fiber fraction is equal, the predicted tensor orientation would be exactly between the two actual fiber populations, resulting in significant error relative to either population (40° in this case). (*B*) Output graph of the DTI simulated experiment depicting the change of the principal eigenvector of the diffusion tensor in response to varying the relative angular orientation of the two intrinsic myofiber populations of the tongue. If the transversus muscle is defined to lie along the x axis in a standard Cartesian x-y coordinate system and the verticalis muscle orientation is varied from 45 to 135° the orientation of the diffusion tensor's principal eigenvector will jump from 45 to 135° as the verticalis muscle orientation passes through 90°. This phenomenon is due to the fact that the principal eigenvector will bisect the acute fiber crossing angle, and explains the toggling nature of the octahedra in our DTI data.

Viewed from the perspective of the whole muscle, DTI effectively depicts regions of high and low anisotropy, a fact which may have particular relevance when considering the behavior of tissue during various conditions, such as stimulated proliferation or pathological remodeling. DTI is most accurate in resolving fiber direction and in defining constituent fiber populations, when the tissue is most spatially homogeneous, i.e., possess high diffusion anisotropy, whereas the resolution of fiber direction by DTI is more limited in tissues whose fiber populations are spatially heterogeneous, i.e., possess low diffusion anisotropy. The exact definition of fiber orientation in spatially heterogeneous tissues is most aptly discerned by microscopic methods, with the ability to discriminate spatially dissimilar fiber populations. The combination of DTI and two-photon microscopy, therefore, provides a robust method for charac-

terizing heterogeneous architectural environments in biological tissues, inasmuch as structural organization can be considered at varying length scales in the same specimen.

Limitations in the current DTI technique may be improved significantly in future studies. If we assume a diffusion time on the order of 100 ms (as calculated from the EPI pulse sequence), and diffusivity of 2.2×10^{-3} mm^2/s which is typical of skeletal muscle, the r.m.s. diffusion length ($\mathbf{x}_{rms} = \sqrt{2\mathbf{D}t}$) is ~20 μm. This relatively short diffusion length would most likely limit proton movement through the semi-permeable sarcolemma of the myofibers, which are 20 to 80 μm in diameter, thereby mitigating the distinction between aligned and fiber patches and continuously interwoven fiber network. Further experiments may take advantage of longer mixing times in the DTI pulse sequence to ascertain the properties of the diffusion tensor (anisotropy, orientation) at varying diffusion times. Longer diffusion times should increase tensor anisotropy as fiber barriers are encountered by a greater number of protons diffusing orthogonal to the long axis, while motion along the fiber axis remains less restricted (Basser, et al., 1994). Extracellularly, proton displacement should also be more anisotropic at longer diffusion times. Movements across and through the myofiber patches would be hindered to a greater degree than displacements along the axes of individual fibers. Thus the second eigenvector of the diffusion tensor may point across the myofiber patch (orthogonal to the fiber direction) or orthogonal to both the fiber direction and patch plane. The extent to which diffusion is affected by the stoma of blood vessels or nerves surrounding the fibers is also unknown. With our current voxel resolution, this latter question is difficult to answer, as a single voxel may have multiple heterogeneously aligned patches, and DTI accounts only for the mean diffusivity within that voxel. Therefore, to answer this question, DTI voxels need to be co-registered precisely with the microscopic field-of-view and the two must be conceived on similar length scales.

In conclusion, we have used two complementary imaging techniques, DTI and two-photon microscopy, to resolve the heterogeneous microscopic structure of the core region of the mammalian tongue. This study has provided data supporting a novel formulation of lingual myoarchitecture, emphasizing the relationship between individual fibers and fiber bundle sheets in constituting the tissue. We propose that the use of these imaging modalities, in concert, provide a means for understanding complex three-dimensional structural relationships in tissues with heterogeneously oriented fibers and fiber bundles.

REFERENCES

Basser, P. J. 1995. Inferring microstructural features and the physiological state of tissues from diffusion-weighted images NMR in Biomedicine. *NMR Biomed.* 8:333–344.

Basser, P. J., J. Mattiello, and D. LeBihan. 1994. MR diffusion tensor spectroscopy and imaging. *Biophys. J.* 66:259–267.

Centonze, V. E., and J. G. White. 1998. Multi-photon excitation provides optical sections from deeper within scattering specimens than confocal imaging. *Biophys. J.* 75:2015–2024.

Denk, W., J. H. Strickler, and W.W. Webb. 1990. Two-photon laser scanning fluorescence microscopy. *Science.* 248:73–6.

Gilbert, R. J., T. G. Reese, S. J. Daftary, R. N. Smith, R. M. Weisskoff, and V. J. Wedeen. 1998. Determination of lingual myoarchitecture in whole tissue by NMR imaging of anisotropic water diffusion. *Am. J. Physiol.* 275:G363–369.

Le Bihan, D. 1995. Molecular diffusion, tissue microdynamics and microstructure. *NMR Biomed.* 8:375–386.

Masters, B., P. T. C. So, and E. Gratton. 1997. Multiphoton excitation fluorescence microscopy and spectroscopy of in vivo human skin. *Biophys. J.* 72:2405–2412.

Miller, A. J. 1982. Deglutition. *Physiol. Rev.* 62:129–184.

Miyawaki, K. 1974. A study of the musculature of the human tongue. Annual Bulletin of the Research Institute of Logopedics and Phoniatrics, University of Tokyo 8:23–50.

Mu, L., and I. Sanders. 1999. Neuromuscular organization of the canine tongue. *Anat. Rec.* 256:412–424.

Napadow, V. J., Q. Chen, V. J. Wedeen, and R. J. Gilbert. 1999a. Biomechanical basis for lingual muscular deformation during swallowing. *Am. J. Physiol.* 40:G695–G701.

Napadow, V. J., Q. Chen, V. J. Wedeen, and R. J. Gilbert. 1999b. Intramural mechanics of the human tongue in association with physiological deformations. *J. Biomech.* 32:1–12.

Reese, T. G., R. M. Weisskoff,, V. J. Wedeen. 1998. Diffusion NMR facilitated by a refocused eddy-current EPI pulse sequence. *In* Proceedings of the International Society for Magnetic Resonance in Medicine, Sixth Annual Meeting. vol.1, p.663.

Russ, J. 1999. The Image Processing Handbook, CRC Press, Boca Raton, FL.

Smith, K. K., and W. M. Kier. 1989. Trunks, tongue, and tentacles: moving with skeletons of muscle. *Am. Scientist.* 77:29–35.

Van Doorn, A., P. H. M. Bovendeerd, K. Nicolay, M. R. Drost., J. D. Janssen. 1996. Determination of muscle fibre orientation using diffusion-weighted MRI. *Eur. J. Morphol.* 34:5–10.

Wedeen, V. J., T. G. Reese, V. J. Napadow, and R. J. Gilbert. 2001. Demonstration of primary and secondary muscle fiber architecture of the bovine tongue by diffusion tensor MRI. *Biophys. J.* 80:1024–1028.